Dynamical correlation functions in a one-dimensional Ising-like antiferromagnetic $CsCoCl_3$: A neutron scattering study

H. Yoshizawa* and K. Hirakawa
The Institute for Solid State Physics, The University of Tokyo, Roppongi, Minato-ku Tokyo 106, Japan

S. K. Satija and G. Shirane
Brookhaven National Laboratory, Upton, New York 11973
(Received 20 May 1980)

Spin dynamics in a one-dimensional (1D) antiferromagnet $CsCoCl_3$ is studied by inelastic neutron scattering. We report the first experimental evidence for a propagative mode of 1D antiferromagnetic domain walls predicted by Villain. Instead of a usual Lorentzian line shape, a characteristic shoulder can be seen in $S_{zz}(q,\omega)$ near $\omega=0$ for $q \gtrsim \kappa$. This shoulder appears only at elevated temperatures, which indicates that the shoulder intensity corresponds to the number of thermally activated domain walls. The 1D antiferromagnet domain-wall motion can also affect the spin-wave spectrum as shown by theoretical calculation of Ishimura and Shiba. The observed spectrum consists of the excitation continuum of nondegenerate magnon states due to the motion of 1D antiferromagnet domain walls. Using the dispersion formula $\hbar\omega_q = 2J(1-8\epsilon^2\cos^2 qc)$, we evaluate the exchange $2J$ and ϵ to be 12.75 ± 0.1 meV and 0.14 ± 0.02, respectively. These values can describe both the boundaries of the excitation continuum $2J \pm 4\epsilon J|\cos qc|$ and the shoulder position in $S_{zz}(q,\omega)$, $4\epsilon J|\sin qc|$, correctly. The asymmetry of the spin-wave line shapes with heavy spectral density towards the lower-energy side, is, however, more enhanced than the theoretical prediction.

I. INTRODUCTION

The spin dynamics in one-dimensional (1D) magnetic systems with $S=\frac{1}{2}$ has been studied extensively during the past decade.[1] In particular, the spin-wave excitation spectrum observed in a 1D Heisenberg antiferromagnet $CuCl_2 \cdot 2N(C_5D_5)$ (CPC)[2,3] has shown several unique features attributable to the quantum nature of this system. For a 1D planar ferromagnet $CsNiF_3$,[4] the careful study of the line shapes of the longitudinal spin correlations has indicated the existence of the so-called solitons in the presence of static magnetic field. Because of these nonlinear aspects, it is important to study the spin dynamics in the 1D magnetic materials with $S=\frac{1}{2}$. In this context, a 1D Ising-like antiferromagnet is one of the most interesting systems,[5,6] whose spin dynamics can be described by the following Hamiltonian:

$$H = 2J\sum_i [S_i^z S_{i+1}^z + \epsilon(S_i^x S_{i+1}^x + S_i^y S_{i+1}^y)] = H_{zz} + H_{xy} , \quad (1)$$

where ϵ denotes the ratio of an additional transverse exchange interaction to the dominant Ising term. The characteristic features of the spin dynamics in the 1D Ising-like antiferromagnet result from the propagation of the antiferromagnetic domain walls due to the small transverse-exchange term H_{xy}. In Fig. 1(a) we illustrate the 1D antiferromagnetic domain walls by broken lines, which are essentially domain boundaries between the two possible antiferromagnetic Néel states. Nonvanishing matrix elements between the neighboring domain walls such as $\langle i|H_{xy}|i+2\rangle \neq 0$ cause the collective mode of the domain-wall motion.

Both the spin-relaxation mechanism and the spin-wave excitations are affected by such domain-wall motions. A few years ago, Villain[5] predicted that the relaxation process in the Ising-like antiferromagnet will be governed by the propagative mode of the domain walls at low temperatures. Instead of a usual diffusive peak in the pure Ising system, two peaks appear around $\hbar\omega=0$ in the neutron scattering function $S_{zz}(q,\omega)$. The peak positions and the cutoff frequency of such a mode are given by $\hbar\Omega_q = 4\epsilon J|\sin qc|$. This mode is shown as the limit of the central component in Fig. 1(b). In contrast to the dispersion relation for Ising-like antiferromagnet which shows a large gap at the zone center, the mode predicted by Villain is gapless and its cross section shows a sharp cutoff at frequency $\hbar\Omega_q$. Villain[5] has noted that the picture of this mode fails for the smaller wave vector $q \lesssim \kappa$ due to collisions among the propagative domain walls. However, the linewidths for $q \lesssim \kappa$ are of the order $\kappa\epsilon J$ which is broader than what one expects from thermally activated relaxation process in a pure Ising antiferromagnet. Recently, Ishimura and

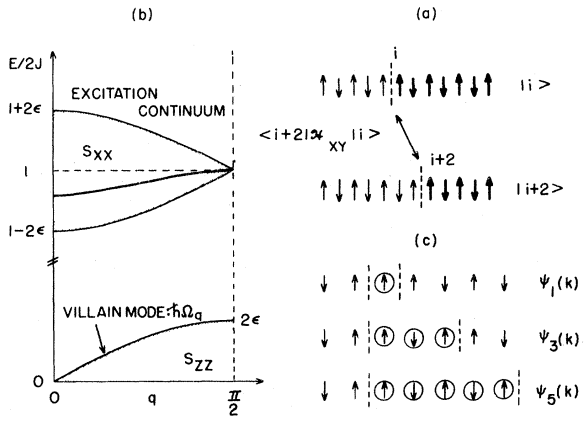

FIG. 1. (a) 1D antiferromagnetic domain walls are shown schematically. Two broken lines represent the domain walls which can move to neighboring positions, for example, from i to $i+2$ due to the transverse matrix element $\langle i+2|H_{xy}|i\rangle$. (b) Schematic illustration of the spin-wave excitation continuum and the Villain mode ($\hbar\Omega_q$). Both have the bandlike cross sections extending up to 2ϵ (dotted regions). The thick line in the continuum corresponds to the peak position of the spectral weight derived by Ishimura and Shiba in Ref. 6. (c) A spin-wave excitation creates domain-wall pair states $\psi_1(k)$, $\psi_3(k)$, $\psi_5(k)$, etc., which are degenerate in the pure Ising limit. The domain-wall motion lifts this degeneracy and causes the excitation continuum.

Shiba[6] (IS) have demonstrated by numerical calculations that the line shapes of $S_{zz}(q,\omega)$ near the zone boundary really show the sharp shoulders at the appropriate temperatures.

The effect of the domain-wall motion on the spin-wave spectrum is also striking. In the Ising-like system, the spin-wave excitation $\psi_1(k)$ as shown at the top of Fig. 1(c) always accompanies two domain walls. The motion of these domain walls lifts the degeneracy among a large number of domain-wall pair states such as $\psi_1(k)$, $\psi_3(k)$, $\psi_5(k)$, etc. In consequence, the simple Ising spectrum is replaced by the excitation continuum of the domain-wall pair states,[6] which extends from $-4\epsilon J$ to $4\epsilon J$ around $2J$ at the zone center. Whereas at the zone boundary, the width of the excitation continuum remains sharp because matrix elements of the type $\langle\psi_1(k)|H_{xy}|\psi_3(k)\rangle$, etc., vanish at that point. Such a continuum of excitations is depicted in Fig. 1(b). Moreover, Ishimura and Shiba[6] have pointed out that the des Cloiseaux and Gaudin spectrum, which has been believed to give the true dispersion relation for the 1D Ising-like antiferromagnet, corresponds neither to the lower boundary nor to the peak position of the excitation continuum. Theoretical calculations[6] have also shown that in 1D Ising-like antiferromagnet, $S_{zz}(q,\omega)$ has a weak side band whose intensity is smaller by a factor of ϵ^2 than that of the $S_{xx}(q,\omega)$ side band. A central component for $S_{xx}(q,\omega)$ is also predicted by the theory.

The purpose of the present paper is to report the first experimental evidence for these quantum effects on the spin dynamics caused by the antiferromagnetic domain-wall motion in the 1D Ising-like antiferromagnet with $S=\frac{1}{2}$. For this purpose we have selected $CsCoCl_3$. This material has been known to behave almost ideally as a 1D Ising-like antiferromagnet with $S=\frac{1}{2}$.[7] Though the weak interchain coupling causes 3D ordering below $T_N=23$ K, the static correlation above 30 K conforms excellently to the exact formula of 1D pure Ising model.[8] Varying estimates of ϵ have been obtained in earlier neutron studies on this compound.[9–11] The order of magnitude of ϵ from these studies is ~ 0.1.

In this paper we report the results of detailed lineshape study of both $S_{xx}(q,\omega)$ and $S_{zz}(q,\omega)$ response functions. In particular, we will deal with the effects of domain-wall motion on these line shapes and compare our experimental results with the recent theoretical calculations of Villain[5] and Ishimura and Shiba.[6] The preliminary results of our study on the spin-wave excitation continuum have been reported recently.[12]

II. EXPERIMENTAL PROCEDURES

The single crystal of $CsCoCl_3$ was prepared in the same manner described previously.[8] This crystal has a hexagonal structure with the space group $D_{6h}^4-P6_3/mmc$. The size of the crystal used in this study is about $10\times15\times4$ mm^3 with the lattice constants $a=7.14$ Å and $c=5.99$ Å. All the measurements were carried out on the triple-axis neutron spectrometers at the Brookhaven High-Flux Beam Reactor. Pyrolytic graphites reflecting from (002) planes were used for monochromator as well as bent analyzer, and the pyrolytic graphite filter was placed after the sample position to remove higher-order neutrons. Most of the scans for the spin-wave measurements were carried out with the fixed outgoing neutron energy $E_f=14.7$ meV, while the final energy E_f was changed to 13.7 meV for the central component measurements. The sample was oriented with the magnetic (hhl) zone as the scattering plane and was mounted in a CT-14 cryostat with the temperature being measured and controlled by a calibrated platinum or germanium resistor. We use the magnetic unit cell with the lattice constants $A=\sqrt{3}a$ and $C=c$ throughout the experiments. The distance c is twice the nearest-neighbor cobalt distance along the c axis. Thus, $qc=\pi$ is the antiferromagnetic zone-center point and $qc=\frac{1}{2}\pi$ is the zone boundary.

Before we proceed with the experimental results, we will explain our strategy to observe the response functions by the neutron scattering technique. In

Fig. 2 we depict the typical profiles of the dynamical response functions $S_{\alpha\alpha}(q,\omega)$ at $q=0.4$ calculated by IS[6] with the parameters appropriate to $CsCoCl_3$. The strongest intensity appears at 13 meV in $S_{xx}(q,\omega)$, which corresponds to the spin-wave excitation. A very weak intensity can be found at the same energy region in $S_{zz}(q,\omega)$. At around $\hbar\omega=0$, we can see the central components of both $S_{zz}(q,\omega)$ and $S_{xx}(q,\omega)$, but the intensity of $S_{zz}(q,\omega)$ is approximately twice that of $S_{xx}(q,\omega)$.

At the bottom of Fig. 2 the magnetic (*hhl*) reciprocal plane is shown, where the arrows represent several scans we have made through the experiments. When the system has an easy axis in the direction of the c axis, the neutron scattering cross section can be written

$$d^2\sigma \propto (\sin^2\phi)S_{zz}(q,\omega)+(1+\cos^2\phi)S_{xx}(q,\omega)\ , \qquad (2)$$

where ϕ is the angle that the scattering vector $\vec{Q}$ makes with the c^* axis. If the scattering vector $\vec{Q}$ is set parallel to the c^* axis, i.e., $\phi=0$, we can observe $S_{xx}(q,\omega)$ exclusively. On the contrary, to see $S_{zz}(q,\omega)$, ϕ should be set as large as possible. However, there is no place where only $S_{zz}(q,\omega)$ can be seen. Therefore, we observe only $S_{xx}(q,\omega)$ in the D scan, while in the A, B, and C scans we observe $S_{zz}(q,\omega)$ and $S_{xx}(q,\omega)$ with roughly equal weights. As seen in Fig. 2, the central component of $S_{zz}(q,\omega)$ may be determined after the contribution of $S_{xx}(q,\omega)$ is subtracted. It may, however, not be possible to observe the side band of $S_{zz}(q,\omega)$ because it is always masked by that of $S_{xx}(q,\omega)$ with at least 100 times stronger intensity.

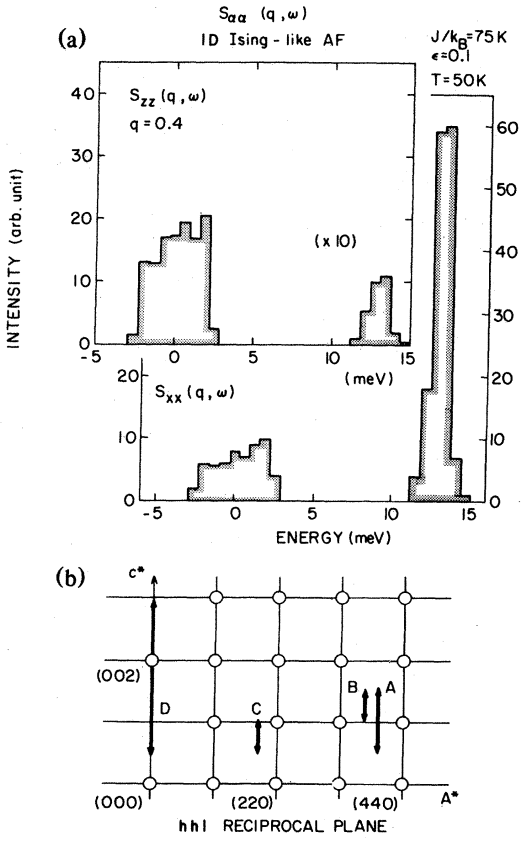

FIG. 2. (a) Theoretical line profiles of the dynamical response functions $S_{\alpha\alpha}(q,\omega)$ in 1D Ising-like antiferromagnet with $q=0.4$. (The zone boundary corresponds to $q=0.5$.) (b) Magnetic *hhl* zone. Arrows indicate the scans performed in the present experiments.

To separate the $S_{zz}(q,\omega)$ component from the $S_{xx}(q,\omega)$ component, we must compare two data taken at the different positions on the scattering plane. Because of the large absorption cross section of $CsCoCl_3$, an effective volume which can contribute to the scattering intensity varies drastically in the scattering plane. The effective volume thus depends on the instrumental configuration, especially on the crystal rotation angle ψ and the scattering angle $2\theta_S$. As a measure of the effective volume, the intensity of the incoherent scattering was observed at high temperatures where the magnetic cross section smears out. The effective volume observed in these scans shows little dependence on the incident energy of neutrons and the most dominant factor was found to be the crystal dimensions seen from the analyzer position.

III. CENTRAL COMPONENT OF $S_{\alpha\alpha}(q,\omega)$

In order to observe the characteristic features of the central components, constant Q scans were carried out at $T=5$ and 50 K along the A, B, C, and D lines in Fig. 2. According to numerical calculations of IS, 50 K is the optimum temperature for observing sufficient intensity in the $S_{\alpha\alpha}(q,\omega)$ central components. Thus we decided to do most of the scans at 50 K. Some limited scans were also made at temperatures of 25, 40, and 80 K. The 5-K scans were done mainly to measure the background levels. Unfortunately, incoherent scattering in $CsCoCl_3$ is very strong and due to the instrumental resolution width extends from -1.0 to 1.0 meV. As seen in Fig. 2, however, we can expect that the magnetic cross section will not vanish up to about 3.0 meV. Therefore, we have tried to look for the central component shoulder in the tail part of the incoherent scattering. The results for $\zeta=0.2$ and 0.4 where $q=(2\pi/c)\zeta$ are shown in Figs. 3 and 4. The strong incoherent scattering seen around $E=0.0$ meV shows little temperature dependence. At the tail part from 1.0 to 4.0 meV, the intensity at $T=50$ K increases clearly from the background level at $T=5$ K. The data have been plotted on a semilog scale to accommodate both the

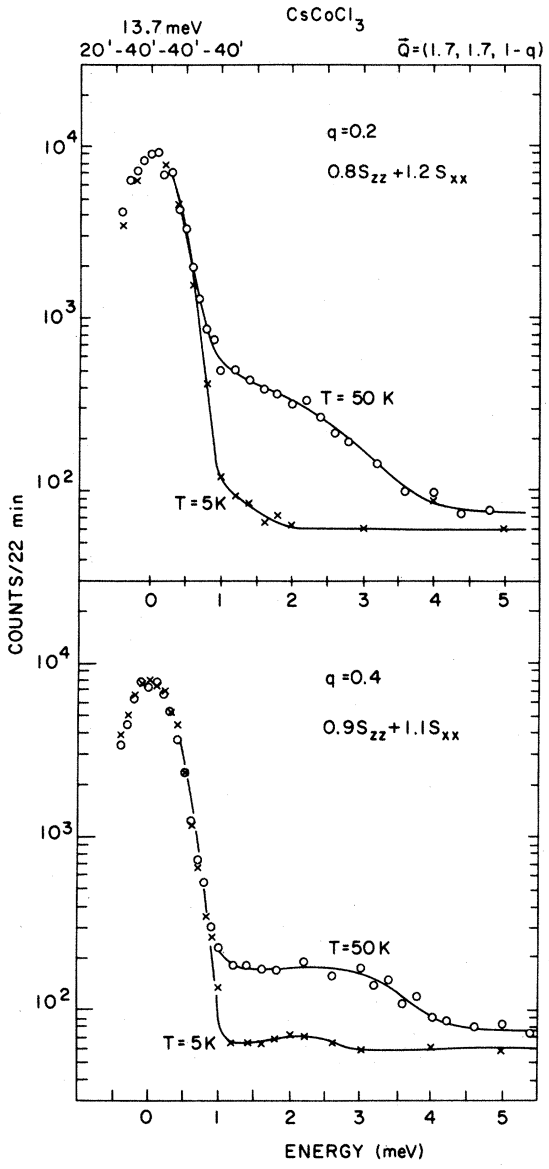

FIG. 3. Neutron profiles observed at $Q=(1.7, 1.7, 1-\zeta)$ with $\zeta=0.2$ and 0.4.

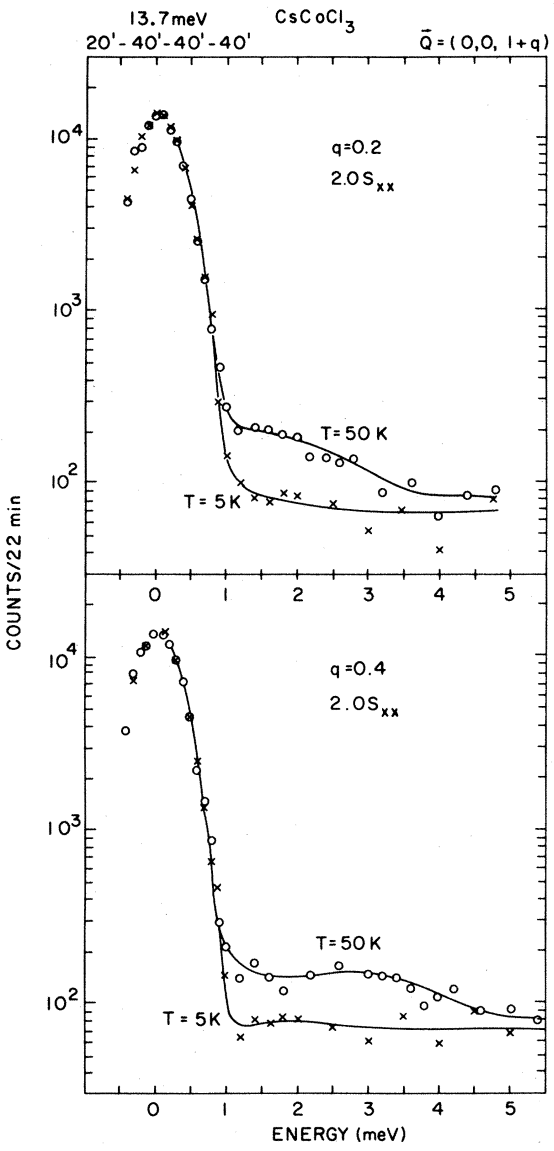

FIG. 4. Neutron profiles observed at $Q=(0, 0, 1+\zeta)$ with $\zeta=0.2$ and 0.4.

large incoherent scattering and the shoulder intensities on the same plot. As the profiles in Fig. 3 were observed at $\vec{Q}=(1.7, 1.7, 1-\zeta)$, they contain both the $S_{zz}(q, \omega)$ and $S_{xx}(q, \omega)$ components. The profiles shown in Fig. 4 were observed at $\vec{Q}=(0, 0, 1+\zeta)$ and contains only the $S_{xx}(q, \omega)$ central component. From these scans, we estimated the contribution of the $S_{xx}(q, \omega)$ component at $\vec{Q}=(1.7, 1.7, 1-\zeta)$ by correcting for the orientation factor, the magnetic form factor, and the effective volume. The resulting cross section shown as the $S_{xx}(q, \omega)$ components in Fig. 5 was approximately equal to 30% of the observed intensity at $\vec{Q}=(0, 0, 1+\zeta)$. Pure $S_{zz}(q, \omega)$ components, as also shown in Fig. 5, were obtained after subtracting the $S_{xx}(q, \omega)$ cross section from the total magnetic intensity at $\vec{Q}=(1.7, 1.7, 1-\zeta)$. The profile for $\zeta=0.4$ exhibits a plateau from 1.0 to 3.0 meV and drops rapidly at higher energies. On the other hand, the profile for $\zeta=0.2$ decreases gradually from 1.0 to 4.0 meV.

Now we show the line shapes of $S_{zz}(q, \omega)$ for $\zeta=0.2$ and 0.4 calculated by IS as histograms[6,13] in Fig. 6, where the line shape of the Villain mode is displayed by a line. The feature of the Villain mode is that it has two poles and a sharp cutoff of the cross

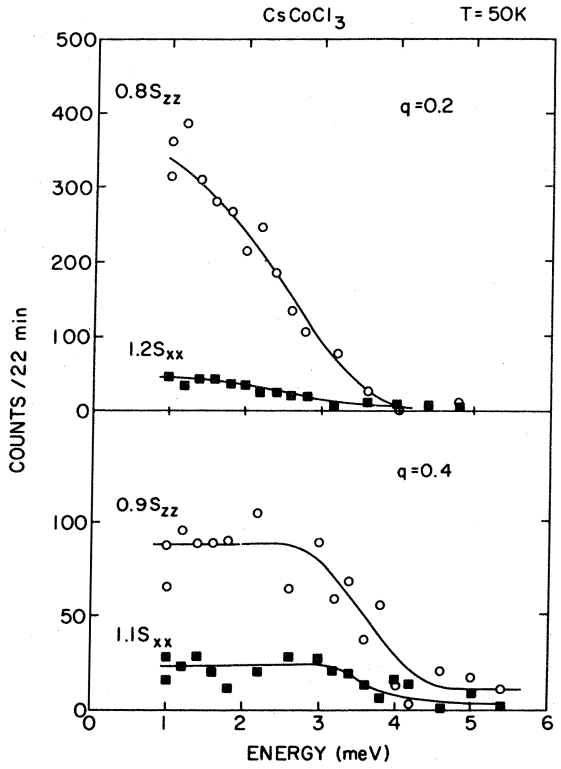

FIG. 5. Wave-vector dependence of central component of $S_{xx}(q,\omega)$ and $S_{zz}(q,\omega)$ after correcting for magnetic form factor and effective volume.

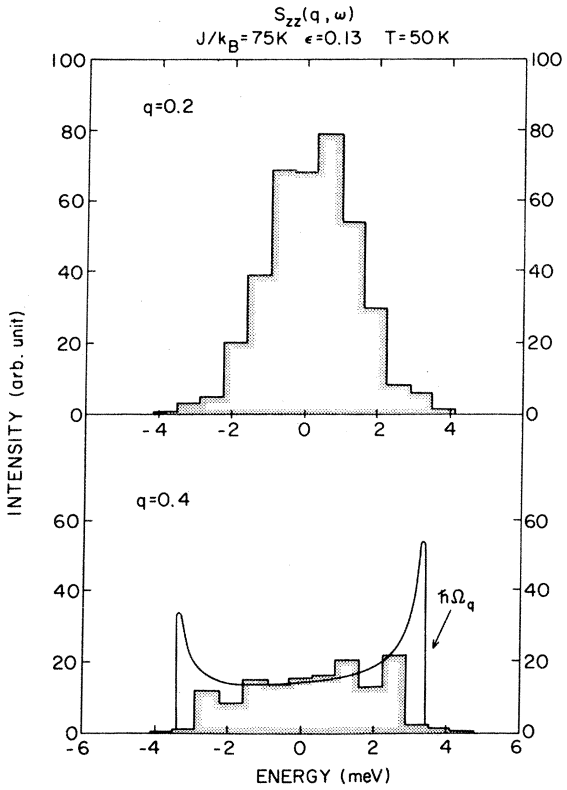

FIG. 6. Calculated profiles of the longitudinal correlation for $CsCoCl_3$ after IS (Refs. 6 and 13). The real line for $\zeta=0.4$ represents the line shape of the Villain mode.

section at the frequency $\hbar\Omega_q$. It is likely that the sharp poles in Villain's theory will be rounded off because of collisions among the propagating domain walls. Thus, the $\zeta=0.4$ histogram with the rectangular line shape, calculated by IS, seems to reflect further the realistic line shape of $S_{zz}(q,\omega)$ in 1D Ising-like antiferromagnet for $q \gtrsim \kappa$. On the other hand, the experimentally observed profile for $\zeta=0.2$ (Fig. 5) does not show any shoulder. However, the line shape for this profile is distinctly different from a Lorentzian. This is because the wave vector $\zeta=0.2$ is not much larger than the inverse correlation length $\kappa=0.15$ at $T=50$ K. As mentioned before, Villain's theory is not applicable in this region.

The wave-vector dependence of experimental line shapes, shown in Fig. 5, agrees very well with the calculation of IS. We also see that the energy where the intensity for $\zeta=0.4$ $S_{zz}(q,\omega)$ vanishes, corresponds approximately to the cutoff energy of the Villain mode $\hbar\Omega_q=4\epsilon J|\sin qc|$. Experimental estimates of J and ϵ are given in Sec. IV. It is worth emphasizing that the square-type line shape seen for this mode is distinctly different from the Lorentzian line shape seen in other magnetic materials. Such a line shape arises from the existence of propagative mode of thermally excited domain walls. We will allude to this point in a little more detail in Sec. V.

A limited number of scans were also made at $\zeta=0.3$ and 0.5. While the $Q=0.5$ scan shows a clear-cut shoulder, the line shape of $q=0.3$ scan resembles that of $q=0.2$ scan. This is in agreement with what one expects theoretically. Earlier neutron results of Hirakawa and Yoshizawa[10] showed the line shapes for $\zeta<0.1$ to be Lorentzian with widths of the order $\kappa\epsilon J$. Thus the line shape for $S_{zz}(q,\omega)$ central component gradually evolves from a square shape at the zone boundary to a Lorentzian at the zone center.

The temperature dependence of the intensity of the $S_{zz}(q,\omega)$ central component also indicates that its origin is due to the thermally excited domain walls. In elevating the temperature, the intensity of the shoulder should increase due to the increase in the number of domain walls. The temperature dependence of the profile for $\zeta=0.4$ was measured in the middle of the plateau, at $\Delta E=2.0$ meV and is shown in Fig. 7. The shoulder intensity increases steeply from 20 to 50 K and remain roughly constant above that temperature. These intensities agree fairly well

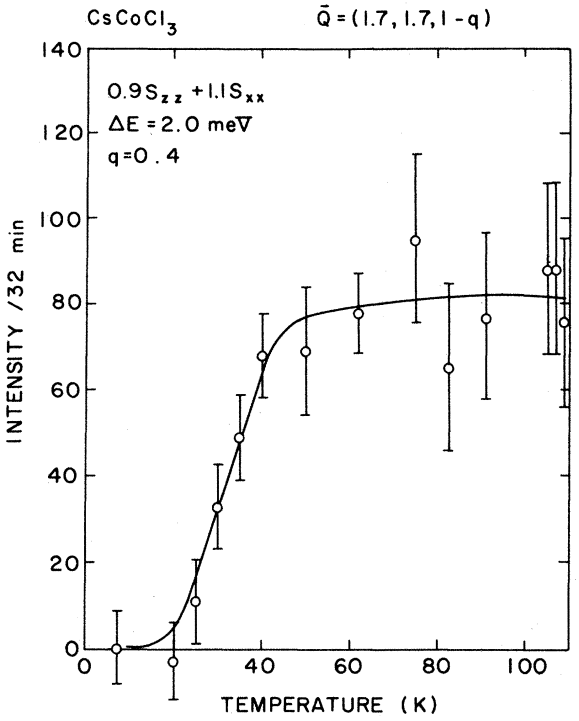

FIG. 7. Temperature dependence of the shoulder intensity, of central component at $\Delta E = 2.0$ meV. The curve is drawn for a guide to the eye.

with the calculations of IS. At higher temperatures, the decrease of correlation length invalidates the Villain mode picture and the line shape changes from square to Lorentzian.

The shape of $S_{xx}(q, \omega)$ central component at $\zeta = 0.4$ is very similar to that of $S_{zz}(q, \omega)$ as also seen in the theoretical calculations. Experimentally seen ratio of intensities of $S_{zz}(q, \omega)$ and $S_{xx}(q, \omega)$ central components are, however, not in agreement with theory. The ratio observed in our experiments is roughly 4:1, while calculation gives a value of about 2:1.

IV. SPIN-WAVE EXCITATION CONTINUUM

In the 1D Ising-like antiferromagnet with $S = \frac{1}{2}$, both the longitudinal and transverse response functions exhibit the central components as well as the side bands. We treated the central components of $S_{zz}(q, \omega)$ and $S_{xx}(q, \omega)$ in Sec. III. In this section we deal with the $S_{xx}(q, \omega)$ side band arising due to spin-wavelike excitations. The $S_{zz}(q, \omega)$ side band is discussed in Sec. V.

We have carried out careful line-shape measurements of the $S_{xx}(q, \omega)$ side band along the $[00\zeta]$ direction to elucidate the nature of the spin-wave excitation continuum due to domain-wall pair states.[6] The results for three different values of momentum transfer at 25 K, which is above the Néel temperature, are shown in Fig. 8. Smoothed experimental line shapes through the whole Brillouin zone are shown in Fig. 9. At the antiferromagnetic boundary, a resolution-limited peak was observed. Upon approaching the zone center, pronounced asymmetry develops towards the higher-energy side and peak positions shift to lower energy. These line shapes confirm the presence of a bandlike excitation. The width

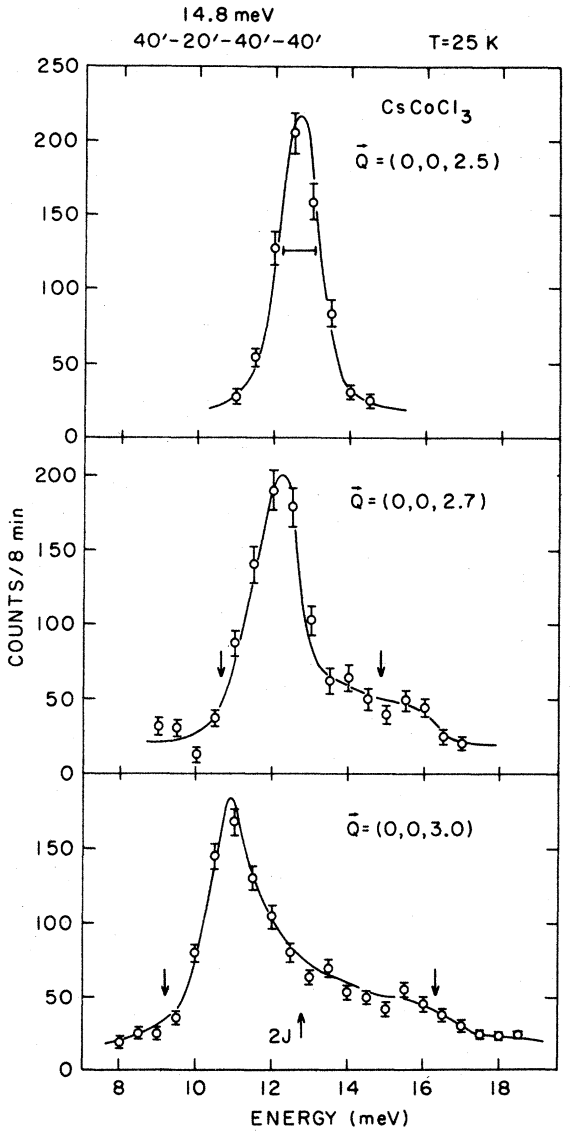

FIG. 8. Constant Q scans at $T = 25$ K showing the spin-wave excitation continuum at three different wave vectors. Arrows indicate the limits of the excitation continuum which corresponds to the broken lines in Fig. 10.

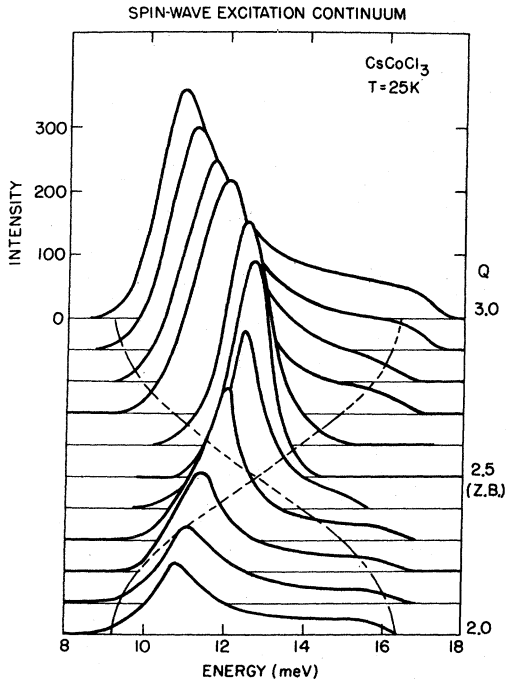

FIG. 9. Smoothed experimental data for Q dependence of the spin-wave excitation continuum observed along $(0, 0, \zeta)$ from $\zeta = 2.0$ to 3.0. Data have been corrected for background and magnetic form factor of Co^{2+}.

of this band is narrowest at the zone-boundary position and most of the spectral weight is concentrated towards the lower-energy side of this band. In Fig. 10 we show the peak positions of $S_{xx}(q, \omega)$ response through the Brillouin zone. In earlier neutron studies on $CsCoCl_3$, the dispersion relation calculated by des Cloizeaux and Gaudin[14] (dCG) was fitted to the experimental peak positions.[9–11] The calculations of IS, however, show that the dCG formula, in contrast with spin-$\frac{1}{2}$ Heisenberg linear antiferromagnet, corresponds neither to the lower limit of the excitation continuum nor to the peak of the spectral density. They have derived the following expression for the peak position:

$$\hbar\omega_q = 2J(1 - 8\epsilon^2 \cos^2 qc) \ , \tag{3}$$

with the boundaries of the continuum extending from $\hbar\omega_q^-$ to $\hbar\omega_q^+$, given by

$$\hbar\omega_q^{\pm} = 2J(1 \pm 2\epsilon \cos qc) \ . \tag{4}$$

Fitting the experimental peak positions to Eq. (3), we get $2J = 12.75 \pm 0.1$ meV and $\epsilon = 0.14 \pm 0.02$. This fit to the experimental data is also shown in Fig. 9. From the experimental point of view, there are two independent quantities which give the value of the parameter ϵ: one is the peak position of the excitation, the other being the spread of the cross section in energy at each wave vector. The calculated boundaries of the excitation continuum using the above values of J and ϵ are shown in Fig. 10 by the dashed lines. Thus at the zone center, the cross section for $S_{xx}(q, \omega)$ side band should extend from about 9 to 16.5 meV. The experimental data shown in Fig. 8 show that the cross section at the zone center does indeed extend from $(2J - 4\epsilon J)$ to $(2J + 4\epsilon J)$.

Recently, Buyers *et al.*[11] have investigated the spin-wave profiles by inealstic neutron scattering. They report that the spin-wave spectrum of $CsCoCl_3$ consists of a sharp peak at the zone boundary, with a broadening of spin-wave profiles at the zone center. This is in agreement with our results. However, the spin-wave spectra reported in their work were not extended much beyond the zone-boundary frequency of 13 meV. As is evident from Fig. 8, the spin-wave cross section at (0,0,3) extends much farther than the zone-boundary frequency of 13 meV. (See Fig. 8.) In order to check that the tail part in the zone-center spectra is magnetic in origin and not arising from any phonon contributions, we made a series of scans along the $[00\zeta]$ direction including points (0,0,1), (0,0,3), and (0,0,5). The line shapes are essentially the same except for the differences in in-

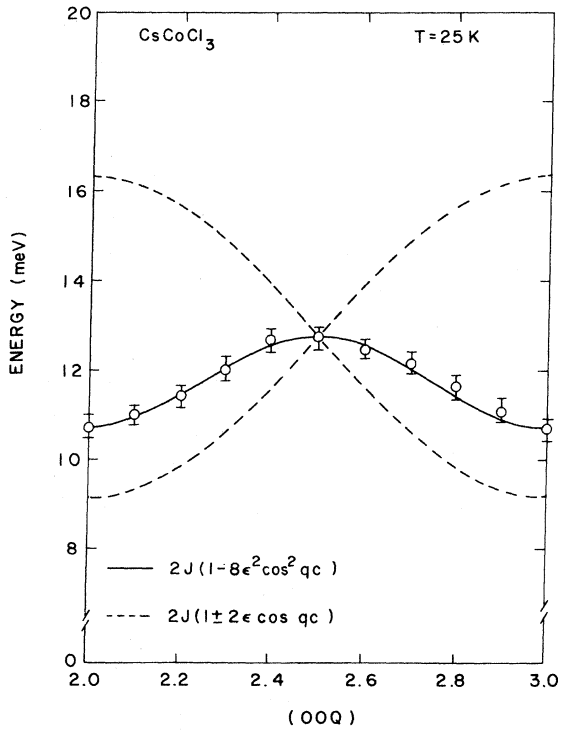

FIG. 10. Spin-wave dispersion relation at $T = 25$ K. Real lines are calculated by Eq. (3), while broken lines represent the upper and lower limits of the excitation continuum calculated by Eq. (4).

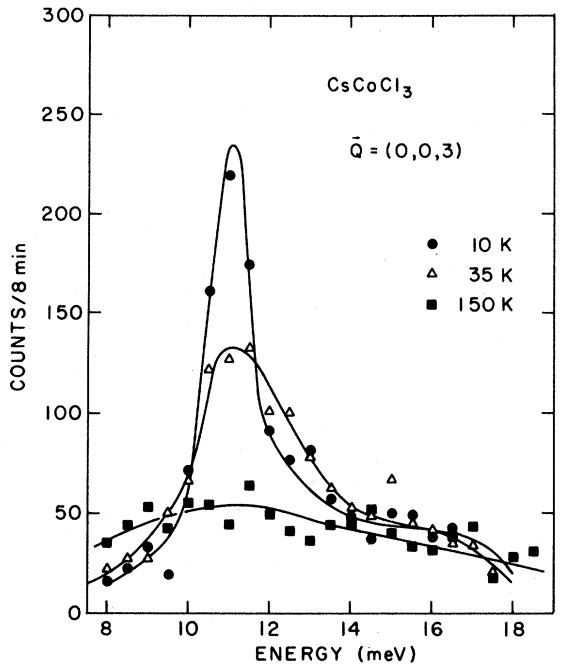

FIG. 11. Temperature dependence of line shapes of the excitation continuum observed at $Q = (0, 0, 3)$.

tensity due to the magnetic form factor of the cobalt. The tail part, if it were arising due to some phonon, should increase as Q^2 and would be much more pronounced in the scan at (0,0,5). Other scans made at (0.6,0.6,1), (1.2,1.2,1), and (1.8,1.8,1) also show the same line shape as the one at point (0,0,1).

One can see in Fig. 9 that the intensity at the nuclear zone center $Q = 2.0$ is weaker than that at the magnetic zone center $Q = 3.0$, where the 1D momentum transfers are equivalent. In the case of the isotopic Heisenberg antiferromagnet, the structure factor of the spin-wave excitation diminishes towards the nuclear Bragg reflection, while in the case of the Ising antiferromagnet, it does not depend upon the scattering vector $\vec{Q}$. For our sample $CsCoCl_3$, the small transverse exchange term H_{xy} causes to reduce the intensity of the spin-wave excitation continuum around (0,0,2), and the ratio of the intensity at (002) against (003) is estimated to be $I(002):I(003) \approx 1:4$, which is much enhanced than the predicted value 1:2 in the calculations of IS.[6,13]

The temperature dependence of the profile at the zone center (0,0,3) is shown in Fig. 11. As the temperature is raised, the asymmetry of the profile reduces. However, the essential features of the profile do not change in going from 10 to 35 K through $T_N = 23$ K. While there is some change in the asymmetry of the profile in going through T_N, the spectra taken at 25 and 35 K look essentially the same. We therefore believe that the effect of interchain interaction in the spectra at 25 K is minimal and does not change substantially on going from 25 to 35 K. However, as we discuss it in Sec. V, even a very small interchain interaction, of the order of $J'/J \approx 10^{-2}$, can enhance the asymmetry in the line shape of the spin-wave spectra.[15] Also, the tail part, if it were arising from any phonon contribution, should have shown a marked increase in going from 10 to 150 K. We can thus conclude that the observed scattering intensity is magnetic in origin. The asymmetry, as mentioned above, arises from the presence of domain-wall pair states giving rise to the spin-wave excitation continuum.

V. DISCUSSION

As we have seen in Secs. III and IV, the essential features of the dynamical response functions in $CsCoCl_3$ can be explained satisfactorily by numerical calculations of IS.[6,13] Namely, the domain-wall propagation causes the non-Lorentzian line shape in the longitudinal correlation function with wave vector near the zone boundary at high temperatures, while an excitation continuum appears in the transverse correlation functions.

As for the $S_{xx}(q, \omega)$ side band, Eqs. (3) and (4) give the best estimation of the Hamiltonian parameters J and ϵ. The spectral weight is heavily concentrated towards the lower-energy side of the spin-wave continuum. However, the exact line shape observed experimentally does not agree very well with the calculations of IS. They calculated a very broad asymmetric peak at the zone center with gradually decreasing intensity on the high-energy side. Experimentally, we observe an asymmetric and almost double-peaked structure as shown in Fig. 8. It is possible that extending the calculation to higher order in ϵ may give better agreement with experimental results. Another possible source of discrepancy between experiment and theory may be due to the neglect of molecular field arising from a small interchain magnetic interaction. In fact, very recent calculations of Shiba[15] show that asymmetry in the spin-wave profile indeed gets enhanced upon introducing a small interchain interaction. Thus asymmetric spin-wave profiles observed are in agreement with the 1D Ising-like character of this material. A small interchain interaction ($\sim 10^{-2}$), however, enhances the asymmetry of the peaks. The intensity of the side band everywhere in the *hhl* zone can be explained by the $S_{xx}(q, \omega)$ component only. We estimate that the intensity of the $S_{zz}(q, \omega)$ side band is less than one-fourth of the S_{xx} component. The experimental ratio of the relative intensity of central component to the side band in $S_{xx}(q, \omega)$ response at $\zeta = 0.4$ is equal to 1:6, which is in good agreement with calculation of IS.

One of the most interesting features of 1D Ising-like antiferromagnets is the elementary excitations giving rise to the domain walls as shown in Fig. 1(a). Nonvanishing matrix elements of the type $\langle i|H|i+2\rangle$, produce a propagation of the domain walls whose dispersion relation is given by[5]

$$\hbar\omega_k = J + 2\epsilon J \cos 2k \quad . \tag{5}$$

The central component of the longitudinal response $S_{zz}(q,\omega)$ results from the scattering of such states by neutrons. We note that the central component intensity should increase with temperature because of an increase in the number of thermally excited propagating domain walls.

The cutoff frequency for such a process, $\hbar\Omega_q$, given by Villain can be understood in the following manner. At a given momentum transfer $q(=k'-k)$, the neutron scatters the domain-wall state propagating with momentum k to one with momentum k'. In the case of $q=0$, there is no energy as well as momentum transfer, i.e., $\Delta E(q=0)=0$. The energy transfer for $qc=\frac{1}{2}\pi$, will be given by

$$\begin{aligned}\Delta E(qc=\tfrac{1}{2}\pi) &= E(k') - E(k) \\ &= E(k-\tfrac{1}{2}\pi) - E(k)\end{aligned} \tag{6}$$

with k ranging from 0 to π. This can take any value from 0 to $4\epsilon J$ as seen from Eq. (6). The minimum and maximum energy transfer at any arbitrary momentum transfer q is thus $\hbar\Omega_q=0$ and $\hbar\Omega_q = 4\epsilon J|\sin qc|$, respectively. Therefore, at $q \gtrsim \kappa$, one expects to see a continuum of energies from $E=0$ to $4\epsilon J|\sin qc|$. Experimentally observed width in $S_{zz}(q,\omega)$ response validates this picture.

The central component in $S_{xx}(q,\omega)$ response function also arises from a similar mechanism. The $S_{xx}(q,\omega)$ response corresponds to a one spin-flip process, i.e., $\Delta S_z = \pm 1$. One can see from Fig. 1(a) that the domain-boundary spin has two nearest-neighbor spins such that one is parallel and the other one antiparallel ($\uparrow\uparrow\downarrow$). Therefore, the molecular field on the domain-boundary spin cancels out and the one spin-flip process causes the $S_{xx}(q,\omega)$central component. It should be noted that this process changes two successive up spins ($\uparrow\uparrow$) to two successive down spins ($\downarrow\downarrow$). If we call the former the domain-wall propagating state, then we can call the latter an anti-domain-wall propagating state. Thus we can interpret the $S_{xx}(q,\omega)$ central component as the scattering process between domain-wall and anti-domain-wall propagating states ($\uparrow\uparrow \leftrightarrow \downarrow\downarrow$). The scattering cross sections of both $S_{zz}(q,\omega)$ and $S_{xx}(q,\omega)$ extend from $E=0$ to the cutoff value $\hbar\Omega_q$ and exhibit shoulders near the zone boundary.

In summary, we have established the effects of the collective motion of domain walls in the 1D Ising-like system. The domain-wall motion distorts the line shape of the central component of the longitudinal correlations $S_{zz}(q,\omega)$ and gives rise to the shoulder structure near the zone boundary. In addition, we observe the shoulder in the $S_{xx}(q,\omega)$ central component and we have noted that the propagative domain-wall picture can also explain the characteristic line shape in the transverse correlations $S_{xx}(q,\omega)$ which appears near the zone boundary. The spin-wave excitations in $S_{xx}(q,\omega)$ consists of a continuum of the excited states instead of an isolated branch given by dCG. Although the dispersion relation and the continuum boundaries can be well described by IS formulas, the asymmetry of the profile is much enhanced especially below T_N(23 K). This asymmetry may be arising due to the effect of a molecular field created by a weak interchain coupling. The central component of the transverse response $S_{xx}(q,\omega)$ also shows a shoulder even at the zone center, which the calculations of IS do not predict.

ACKNOWLEDGMENTS

This work was carried out while one of us (H.Y.) was a guest at Brookhaven National Laboratory, whose hospitality he gratefully acknowledges. We are indebted to N. Ishimura and H. Shiba for helpful discussions and for providing the results of numerical calculations used in this study. We are grateful to G. F. Reiter for stimulating discussions on this subject and to W.J.L. Buyers for exchange of useful information on experimental conditions. The research at Brookhaven was supported by the Division of Basic Energy Sciences, U.S. DOE, under Contract No. DE-AC02-76CH00016.

---

*Guest at BNL.

[1]M. Steiner, J. Villain, and C. G. Windsor, Adv. Phys. 25, 87 (1976).

[2]Y. Endoh, G. Shirane, R. J. Birgeneau, P. M. Richards, and S. L. Holt, Phys. Rev. Lett. 32, 4, 170 (1974).

[3]I. U. Heilmann, G. Shirane, Y. Endoh, R. J. Birgeneau, and S. L. Holt, Phys. Rev. B 18, 3530 (1978).

[4]J. K. Kjems and M. Steiner, Phys. Rev. Lett. 41, 1137 (1978).

[5]J. Villain, Physica (Utrecht) B 79, 1 (1975).

[6]N. Ishimura and H. Shiba, Prog. Theor. Phys. 63, 743 (1980).

[7]N. Achiwa, J. Phys. Soc. Jpn. 27, 561 (1969).
[8]H. Yoshizawa and K. Hirakawa, J. Phys. Soc. Jpn. 46, 448 (1979).
[9]U. Tellenbach, J. Phys. C 11, 2281, 2287 (1978).
[10]K. Hirakawa and H. Yoshizawa, J. Phys. Soc. Jpn. 46, 455 (1979).
[11]W. J. L. Buyers, J. Yamanaka, S. E. Nagler, and R. L. Armstrong, Solid State Commun. 33, 857 (1980).
[12]S. K. Satija, G. Shirane, H. Yoshizawa, and K. Hirakawa, Phys. Rev. Lett. 44, 1548 (1980).
[13]N. Ishimura and H. Shiba (private communication). Line shapes shown in Fig. 6 were recalculated with the best estimated value of $\epsilon = 0.13$ instead of $\epsilon = 0.1$ in Ref. 6.
[14]J. des Cloizeaux and M Gaudin, J. Math. Phys. 7, 1384 (1966).
[15]H. Shiba (unpublished).